View Online / Journal Homepage / Table of Contents for this issue
Dynamic Article Links

PCCP

Cite this: *Phys. Chem. Chem. Phys.*, 2011, **13**, 6053–6058

www.rsc.org/pccp

PAPER

Theoretical investigation of formation mechanism of bipyridyl molecule on Ni(111) surface: implication for synthesis of N-doped graphene from pyridine

Hui Feng, Zhaosheng Qian,* Chen Wang, Congcong Chen and Jianrong Chen

Received 8th November 2010, Accepted 20th January 2011
DOI: 10.1039/c0cp02441d

The formation mechanism of bipyridyl molecule catalyzed by nickel catalyst with pyridine precursor has been studied using density functional theory calculations. The formation of bipyridyl on Ni(111) surface from two pyridine molecules is considered as the initial process of N-doped graphene growth, and the minimum energy pathway for the formation has been investigated in detail. The whole formation processes mainly includes three steps, *i.e.*, the dehydrogenation of the first pyridine, adsorption and dehydrogenation of the second pyridine, and formation of the bipyridyl molecule. It is found that the C–H bond of pyridine could be selectively dissociated while the C–C and C–N bond connections are retained during the catalytic processes. The N-doped graphene formed by pyridine only contains pyridine-like nitrogen atoms, suggesting a possible way to produce N-doped graphene with pure pyridine-like nitrogen atoms. The comparison of formation mechanisms between bipyridyl and biphenyl molecules was carried out, and the results imply a lower temperature process for synthesis of N-doped graphene from pyridine than that for graphene from benzene.

Introduction

Graphene, a single layer of graphite where the carbon atoms are arranged in a hexagonal lattice structure, has attracted a great deal of interest due to its unique electronic and physico-chemical properties and potential applications in various fields.[1] Many synthesis methods for graphene sheets, including thermal decomposition,[2] micromechanical cleavage,[3] chemical reduction of graphene oxide[4] and confined self-assembly approach[5] have been developed. Graphene exhibits electronic properties and thus has been considered as one of the most promising material for future nanoelectronics.

However, it has recently been found that nitrogen-doped graphene has even better properties in gas sensing, electrical properties, electrochemical biosensors and electrocatalysis. Wei *et al.*[6] synthesized N-doped graphene and found that doping of nitrogen can effectively modulate the electrical properties of graphene. N-Doped graphene has also displayed high electrocatalytic activity for reduction of hydrogen peroxide and fast direct electron transfer kinetics for glucose oxidase.[7] Qu *et al.*[8] found that N-doped graphene can act as an efficient metal-free electrocatalyst for oxygen reduction in fuel cells. The reversible discharge capacity of N-doped graphene is almost double that of pristine graphene.[9] Palnitkar *et al.* [10] found that N-doped graphene has remarkably low turn-on field emission, which is superior to that of other types of nanomaterials. Pt nanoparticles on N-doped graphene layers exhibit outstanding electrocatalytic activity for methanol oxidation.[11] These excellent results make efficient synthesis methods for N-doped graphene a priority. Currently, N-doped graphene is mainly synthesized by chemical vapor deposition, in which the corresponding precursors are CH_4 and NH_3, which are transformed to N-doped graphene at a very high temperature. With the pyridine as the precursor, N-doped carbon nanotubes were synthesized successfully at a relatively low temperature.[12] Similarly, the formation of N-doped graphene is possible using pyridine as precursor. In formation of N-doped graphene or N-doped carbon nanotubes, it is feasible that pyridine can act as the precursor, and thus the radical growth mechanism from pyridine should be explored. The formation of the bipyridyl molecule is a basic and key step of growth of N-doped graphene and carbon nanotubes, and thus a detailed theoretical study for this mechanism is necessary for exploration of synthesis methods of N-doped graphene from pyridine.

In our previous work, we investigated N-doped carbon nanotubes functionalized by transition metal atoms with density functional theory, and found that the nanocomposite materials have excellent catalytic activity in direct methanol oxidation and oxygen reduction reaction.[13] To explain the experimental observation for growth of CNTs,[14] we proposed and explored the six-membered-ring-based radical mechanism for catalytic growth of carbon nanotubes from benzene

College of Chemistry and Life Science, Zhejiang Normal University, Jinhua City, China. E-mail: qianzhaosheng@zjnu.cn; Fax: +86 579 82282269; Tel: +86 579 82282269

precursor theoretically.[15] In this paper, a theoretical study on the formation of bipyridyl molecule over Ni(111) surface with pyridine precursor has been performed using density functional theory (DFT) calculations with both a cluster model and slab model. The results indicate that the C–H bond of pyridine could be selectively dissociated, forming dehydrogenated C_5N species which can form N-doped graphene sheets on the catalyst surface. The comparison of the formation mechanism between bipyridyl and biphenyl was carried out to provide useful information for the synthesis of N-doped graphene from pyridine.

Computational model and methodology

The calculations were performed at the density functional theory (DFT) level by using the Dmol^3 code.[16] The exchange correlation energy was described by the Perdew–Burke–Ernzerhof functional within the generalized gradient approximation (GGA-PBE). For C and H atoms in the pyridine all-electron basis sets were used, and for the Ni atoms effective core potentials (ECP) were used. The double-numeric basis with polarization functions (DNP) were used for all atoms in the adsorbed and substrate systems. We utilized the k-point sampling scheme of a $2 \times 2 \times 1$ Monkhorst–Pack grid and Methfessel–Paxton smearing of 0.005 hartree. We took a global real space orbital cutoff of the atomic basis sets to be 4.0 Å. Spin polarization was also used to calculate the energies and structural parameters of all models. The convergence criteria for structure optimization and energy calculation were 1.0×10^{-5} for SCF, 2.0×10^{-5} au for energy, 4×10^{-3} au for maximum force, and 5×10^{-4} nm for maximum displacement. The transition state (TS) structure search was performed by the complete LST/QST method.[17]

The Ni(111) surface was represented by using two kinds of models: cluster model and slab model.

(a) Cluster model

The cluster model has been widely used in studies on molecule chemisorption on transition metal surfaces. For pyridine adsorption, the Ni(111) surface was modeled using a two layered Ni_{41} cluster with 25 atoms in the top layer. The Ni–Ni distance was fixed at the bulk value of 2.49 Å which is derived from experimental determination. The calculated lattice constants of the Ni crystal of 0.353 nm with the relaxed model used in this paper is in good agreement with the experimental data of 0.352 nm,[18] which shows that the size of the unit cell employed is suitable.

To validate this fixed cluster model, a Ni_{41} cluster with all Ni atoms relaxed were also calculated for the adsorption of pyridine on Ni(111) for comparison. The corresponding adsorption geometry parameters and energy profile show that both the adsorption geometry parameters and energy profile are close to each other by fixed and relaxed cluster models.

(b) Slab model

The slab model has been successfully applied to investigate surface adsorption in recent years. Geometry optimizations and their energetics have been performed by using periodically repeating super tetragonal unit cells. The Ni(111) surface with an area of 12.46×12.46 Å^2 consists of three layers. The vacuum space between neighboring slabs is set to be 10 Å. During the geometry optimization, the pyridine molecules and the uppermost layer of Ni atoms were allowed to relax and the two other layers of atoms were fixed in the bulk geometry. This three-layered slab model was validated by comparing the adsorption geometry parameters of pyridine on Ni(111) by using slab models with two to five layers. It is seen the corresponding adsorption energies show little change from three- to five-layered models. With the three-layered model, the calculation was further optimized with the k-points of $2 \times 2 \times 1$ and $4 \times 4 \times 1$, which give very similar calculation results. Hence, the k-points of $2 \times 2 \times 1$ and three-layered model were used in this study by considering both the calculation accuracy and the computational limit. Chemisorption energies were computed by subtracting the energy of the optimized gas-phase adsorbate and the nickel cluster from the energy of the optimized adsorbate–metal model complex as follows:

$$\Delta E_{ads} = E_{adsorbate/metal} - E_{adsorbate} - E_{metal}$$

Results and discussion

Adsorption properties

First, we briefly present the results of a systematic adsorption study of pyridine on Ni(111) in order to exhibit possible metastable sites which may be important for the pathway analysis. The different isomers of the adsorption configurations have been considered in our study, the results show that different kinds of adsorption configurations for pyridine through the N-atom and C=C bonds can stably exist. Experimental research[19] investigated the adsorption of pyridine on Ni(111) using high-resolution electron energy loss spectroscopy (HREELS), X-ray photoelectron spectroscopy (XPS), and angular-resolved photoelectron spectroscopy (ARUPS) methods. It is found that the molecular plane is parallel to the surface at low coverage at 120 K, corresponding to π-bonded species. At higher coverage, the molecular plane tilts vertically with respect to the surface, indicating bonding through the N lone pair. In our study, we focused on bipyridyl molecule formation from pyridine dehydrogenation on the Ni(111) surface. According to the experiment, dehydrogenation of pyridine occurs usually at higher coverage and higher temperature. In this case, the pyridine mainly presents a perpendicular adsorption configuration and not a parallel configuration. As a result, the perpendicular adsorption was selected as the beginning step for dehydrogenation of pyridine in our study. For comparison, the parallel adsorption was also calculated and the corresponding geometry parameters are given in Table 2. In this work, our calculation shows that the molecular plane of pyridine can be tilted with respect to the surface. Indeed, the minimum-energy conformation corresponds to a pyridine molecule with a perpendicular orientation on top of a single Ni atom and a yaw angle of 45° aligning the molecular plane along the diagonal of the square unit cell. The corresponding chemisorption energy is 0.60 eV with a bonding

 This journal is © the Owner Societies 2011

Table 1 Comparison of the adsorption geometry parameters of pyridine on Ni(111) surface at top site with fixed and relaxed cluster model

Cluster model	E_{ad}[a]/eV	$d_{Ni-Ni(111)}$[b]/Å	d_z[c]/Å	d_{C-C}[d]/Å	d_{C-N}[d]/Å	d_{C-H}[d]/Å	φ[e]/°
Fixed	0.60	0	2.08	1.396	1.353	1.090, 1.097	90
Relaxed	0.78	0.7	2.00	1.395	1.353, 1.356	1.090, 1.092	90

[a] E_{ad} denotes adsorption energy. [b] $d_{Ni-Ni(111)}$ denotes the distance between the Ni atom directly interacting with pyridine and Ni(111) surface. [c] d_z denotes the distance between adsorbate molecule and metal surface. [d] d_{C-C}, d_{C-N}, d_{C-H}, denote the C–C, C–N and C–H bond lengths, respectively. [e] φ denotes the angle between the adsorbate molecule plane and metal surface.

N–Ni distance of 2.08 Å. The detailed adsorption geometry of pyridine molecule on Ni(111) surface is shown in Table 1. In addition, vibrational frequencies of the adsorbed pyridine were calculated to compare with the available experimental data. The calculated values of C–H and C–C bond vibrational modes of pyridine on Ni(111) are 368 and 191 meV respectively, which are very close to the corresponding experimental values of 370 and 190 meV.[19] The results show that the calculated vibrational frequencies are in agreement with the experiment, and further confirm the perpendicular adsorption of pyridine on Ni surface.

To validate this fixed cluster model, the Ni_{41} cluster with all Ni atoms relaxed were calculated for the adsorption of pyridine on Ni(111) for comparison. The corresponding adsorption geometry parameters and energy profile are shown in Table 1, and one can note that although the reconstruction of Ni atoms of the surface takes place, the adsorption geometry parameters and energy profile are close to each other by fixed and relaxed cluster models, which validates the fixed cluster model using in this work. We selected the cluster model rather than the slab model to calculate the whole reaction path for the consideration of both the accuracy of calculations and limitation of computer resources.

Reaction pathways

The proposed reaction pathways for the formation of bipyridyl on Ni(111) surface from two pyridine molecules is shown in Fig. 1. As depicted in Fig. 1, the formation of bipyridyl is considered to occur as the following three steps. Step 1: the first pyridine molecule adsorbed on Ni surface dehydrogenates to a form pyridyl radical and a hydrogen radical. Step 2: a second pyridine molecule adsorbed on Ni surface dehydrogenates also to form another pyridyl radical and hydrogen radical. In step 3 the pyridyl radicals combine to form a bipyridyl molecule.

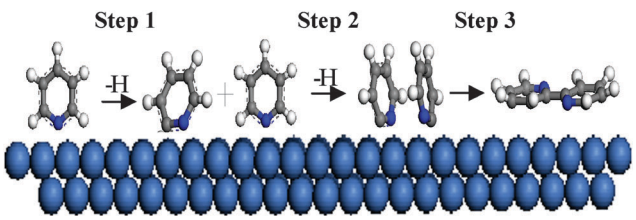

Fig. 1 Three steps of the formation of bipyridyl from pyridine over Ni(111) surface. Step 1: dehydrogenation of the first pyridine molecule upon adsorption on Ni(111) surface. Step 2: dehydrogenation of the second pyridine molecule on Ni(111) surface to form another pyridyl radical. Step 3: combination of two pyridyl radicals to form bipyridyl.

Step 1: Dehydrogenation of the first pyridine molecule to form pyridyl radical

The initial step of the overall reaction pathway is the dehydrogenation of the first pyridine molecule to form a pyridyl radical. Fig. 2 shows the energy profile for the process of dehydrogenation of pyridine from the top site of Ni(111) surface. The geometrical structures of each step are also shown in the figures with top view and side view respectively. First, the pyridine molecule adsorbs on Ni(111) surface. Fig. 2a shows the optimized geometry of pyridine molecule adsorbed on Ni(111) surface, and the corresponding geometry parameters are shown in Table 2. From Fig. 2, we can see that pyridine molecule adsorbs vertically with nitrogen atom downwards on the top site of the Ni(111) surface, which is different with the adsorption geometry of benzene due to the nitrogen atom.[15] The adsorption energy (0.60 eV) is lower than that of benzene (1.18 eV),[15] indicating that benzene adsorbs more easily on Ni(111) surface than pyridine. As is shown in Table 2, the distance between the pyridine molecule and the Ni surface is about 2.08 Å, larger than that for benzene (1.95 Å).[15] The lengths of the C–H bonds neighboring the nitrogen atom of the

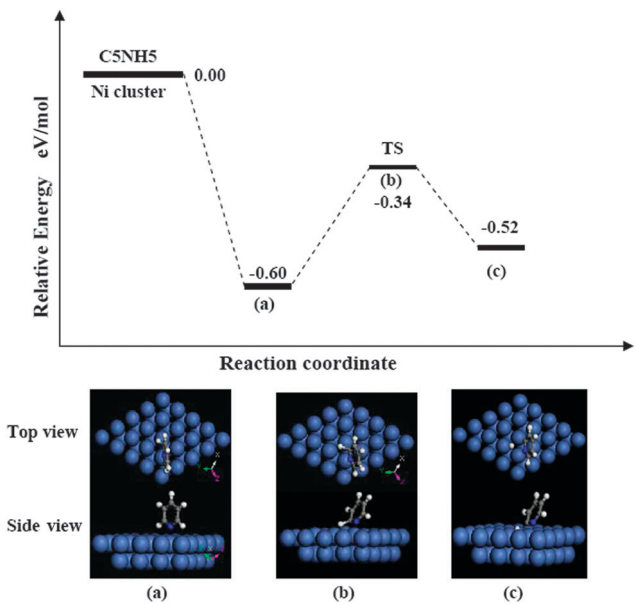

Fig. 2 Energy profile for step 1 corresponding to the first pyridine molecule dehydrogenation on Ni(111) surface with respect to the sum of energies of the free pyridine molecule and the Ni(111) surface. The figures of the top view and the side view of all states along the reactive profile are given in the lower panels with the symmetry of their adsorption site.

Table 2 The adsorption geometry of pyridine, bipyridyl, pyridyl radical and hydrogen radical on Ni(111) surface (cluster model)

System	Site	E_{ad}[a]/eV	d_z[b]/Å	d_{C-C}[c]/Å	d_{C-N}[c]/Å	d_{C-Ni}[c]/Å	d_{N-Ni}[c]/Å	d_{C-H}[c]/Å	φ[d]/°
Pyridine (Fig. 2a)	Top	0.60	2.08	1.396	1.353	2.757	2.08	1.090, 1.097	90
Pyridine	Bridge	1.19	1.96	1.432, 1.459	1.394	1.96	1.96	1.093, 1.099	0
Bipyridyl (Fig. 3h)	Bridge	2.54	2.03	1.429–1.481	1.393, 1.398	2.03	2.03	1.093	0
$C_5NH_4^{\bullet}$ + $H^{\bullet}$ (Fig. 2c)	Bridge	5.25	1.566	1.390, 1.410	1.402, 1.363	1.916	2.082	1.092	60
$C_5NH_4^{\bullet}$ + $H^{\bullet}$ + C_5NH_5 (Fig. 3d)	Bridge (L)	6.57	1.867	1.395, 1.410	1.348	1.865	1.933	1.090, 1.092	60
	Top (R)	—	2.067	1.394, 1.397	1.354	—	2.067	1.090, 1.096	70
$2C_5NH_4^{\bullet}$ + $2H^{\bullet}$ (Fig. 3f)	Bridge (L)	11.34	1.527	1.391, 1.407	1.365	1.977	1.860	1.089, 1.092	90
	Bridge (R)	—	1.534	1.394, 1.405	1.349	1.857	1.989	1.089, 1.092	90

[a] E_{ad} denotes adsorption energy. [b] d_z denotes the distance between adsorbate molecule and metal surface. [c] d_{C-C}, d_{C-N}, d_{C-Ni}, d_{N-Ni} and d_{C-H} denote the C–C, C–N, C–Ni, N–Ni and C–H bond lengths respectively. [d] φ denotes the angle between the adsorbate molecule plane and metal surface. (L) and (R) denote the left and right molecules in figures respectively.

adsorbed pyridine molecule become longer after adsorption. Meanwhile, the C–H bonds far away from the nitrogen atom are unchanged after adsorption. Namely, adsorption is facilitated due to elongation of the C–H bond effected by the catalyst surface through this adsorption mechanism, which means that the C–H bond breaking of pyridine on the metal surface occurs easily leading to dehydrogenation of pyridine by the metal catalyst. Fig. 2c shows the optimized geometry of pyridyl radical and hydrogen radical adsorbed on the metal surface. The pyridyl radical molecule tilts to the bridge site of the Ni(111) surface and the hydrogen radical is adsorbed in the neighbor hollow site, while the tilt angle between the pyridyl molecule and the Ni surface is about 60°.

As shown in Fig. 2b, the geometry of the transition state is that the pyridyl radical molecule adsorbs tilted to the Ni surface in the site between hcp hollow and bridge site of Ni(111) surface. The corresponding geometry parameters of the transition state are shown in Table 3. From Table 3, we can see that pyridyl molecule adsorbs with a title angle of about 60° on the metal surface and the adsorption height is about 1.82 Å. The activation barrier of this dehydrogenation process of the pyridine molecule is about 0.26 eV. However, the calculated gas-phase dehydrogenation barrier is 4.25 eV. This large energy difference between the gas and chemisorbed phases is due to the attractive interaction between the reactants and the metallic surface. Comparing the dehydrogenation activation energies between benzene and pyridine, we can see than the dehydrogenation activation energy for pyridine (0.26 eV) is much smaller than that for benzene (1.16 eV), which may be caused by the introduction of a nitrogen atom in the pyridine molecule, and implies that a lower temperature is needed for dehydrogenation of pyridine than that of benzene.

Step 2: Dehydrogenation of the second pyridine molecule on Ni(111) surface

The energy profile for step 2 is shown in Fig. 3: the second pyridine molecule adsorbs on Ni(111) surface after step 1 and dehydrogenates to form another pyridyl radical and hydrogen radical.

At first, the second pyridine molecule adsorbs on the metal surface. Fig. 3d shows the optimized geometry of the second pyridine molecule together with the pyridyl radical and hydrogen radical obtained in step 1 adsorb on the Ni(111) surface. From Fig. 3, we can see that the second pyridine molecule adsorbs tilted 70° relative to the top site of the Ni surface, while the first pyridyl radical molecule moves to a site between bridge site and hcp hollow site of the Ni surface with a tilt of 60° and the hydrogen radical adsorbs in the neighbor fcc hollow site. The adsorption energy of this process is about 1.32 eV, which is larger than that for benzene (1.03 eV),[15] and is also larger than that for the first pyridine due to the possible influence of the first pyridyl radical. The corresponding geometry parameters are shown in Table 2. The distance between the second pyridine molecule and the Ni surface is about 2.067 Å. The C–H bonds neighboring nitrogen atom of the adsorbed pyridine molecule are also elongated after adsorption. Thus, the elongation of the C–H bond of the pyridine molecule is effected by the catalyst surface through this adsorption mechanism and dehydrogenation of the second pyridine is facilitated by the metal catalyst.

As shown in Fig. 3e, the adsorption geometry of the transition state (TS2) shows the second pyridine molecule titled to the fcc hollow site with the angle of 75° and the corresponding geometry parameters of this transition state (TS2) are shown in Table 3. The second pyridine molecular

Table 3 The adsorption geometry of the transition state on Ni(111) surface

System	Site	d_z[a]/Å	d_{C-C}[b]/Å	d_{C-N}[b]/Å	d_{C-Ni}[b]/Å	d_{N-Ni}[b]/Å	d_{C-H}[b]/Å	φ[c]/°
TS1 (Fig. 2b)	Bridge	1.821	1.392, 1.406, 1.414	1.375	1.949	1.938	1.091, 1.089	60
TS2 (Fig. 3e)	Bridge (L)	1.789	1.393, 1.409, 1.398, 1.435	1.396	1.992	1.900	1.091, 1.089	45
	Bridge (R)	1.907	1.392, 1.404, 1.394, 1.413	1.367	1.863	1.981	1.092, 1.089	75
TS3 (Fig. 3g)	Bridge (L)	1.832	1.422, 1.402	1.354	1.876	1.966	1.094, 1.089	90
	Bridge (R)	1.777	1.398, 1.430, 1.383, 1.391	1.405	2.019	1.851	1.089, 1.100	90

[a] d_z denotes the distance between adsorbate molecule and metal surface. [b] d_{C-C}, d_{C-N}, d_{C-Ni}, d_{N-Ni} and d_{C-H} denote the C–C, C–N, C–Ni, N–Ni and C–H bond lengths respectively. [c] φ denotes the angle between the adsorbate molecule plane and metal surface, (L) and (R) denote the left and right molecules in figure respectively.

 This journal is © the Owner Societies 2011

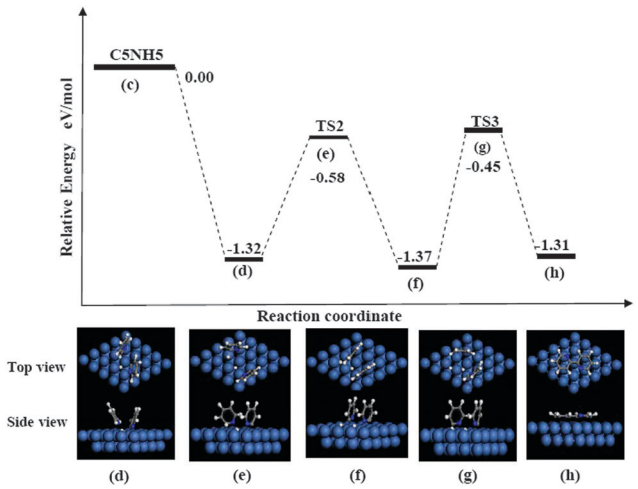

Fig. 3 Energy profile for step 2 corresponding to dehydrogenation of the second pyridine molecule on Ni(111) surface to form another pyridine radical and hydrogen radical. The pyridyl radicals then combine to form bipyridyl. The figures of the top view and the side view of all states along the reactive profile are given in the lower panels with the symmetry of their adsorption site.

plane is rotated to neighbor bridge site of the metal surface and the C–H bond neighboring nitrogen atom becomes longer as the dehydrogenation reaction proceeds. With the breaking of the C–H bond in the second pyridine molecule, the second pyridyl radical and corresponding hydrogen radical form. The activation energy of this process is about 0.74 eV, which is higher than that for the dehydrogenation of the first pyridine molecule, but is much lower than that for benzene (2.94 eV), implying the important role of the nitrogen atom of pyridine.[15] The adsorption geometry of two pyridyl radicals on the metal surface is shown in Fig. 3f. Both the first and the second pyridyl radicals incline to perpendicular adsorption, and the distance between the first and second pyridyl radical and Ni(111) surface are very close.

Step 3: Combination of two pyridyl radicals to form bipyridyl

The radicals formed in step 1 and step 2 are unstable and readily combine with each other. Thee two pyridyl radical molecules both tilt down to metal surface. The top view and side view of the adsorption geometry of the transition state of this process (TS3) is shown in Fig. 3g and the corresponding geometry parameters are shown in Table 3. Eventually the two pyridyl radicals become almost parallel to each other and the distance between the two pyridyl radicals becomes short enough for reaction and the two pyridyl radicals combine to form a bipyridyl molecule. The activation energy of this process is about 0.92 eV, which is close to that for benzene (0.88 eV).[15] Fig. 3h shows the optimized geometry of bipyridyl adsorbed on the Ni(111) surface. The bipyridyl molecule adsorbs parallel on two bridge sites of the Ni(111) surface. The adsorption of bipyridyl also induces a weak sp^3 hybridization including an expansion of the carbon ring from 1.40 to 1.42 Å and an out-of-plane tilt of H atoms of about 9°. The geometry of bipyridyl is a parallel adsorption structure. Accordingly, the formation of bipyridyl from two pyridines in the heterogeneous phase is promoted by the catalytic effects of nickel. The catalytic roles of nickel on this formation are to stabilize the total energy in adsorption of pyridine onto the cluster as well as to weaken the C–H bond strength due to the interaction between H atom and the cluster.

In the formation of the bipyridyl from pyridine, the rate-determining step is the combination of two pyridyl radicals on Ni surface with an activation energy of 0.92 eV. Similarly, in the formation of the biphenyl from benzene, the rate-determining step is the dehydrogenation of the second benzene on Ni surface, whose activation energy is 2.94 eV. Thus, the activation energy of the rate-determining step for formation of bipyridyl molecule is much lower than that for biphenyl molecule, which may imply that a lower temperature can be used for the synthesis of N-doped graphene from pyridine than for pure graphene from benzene. The hydrogen atoms of bipyridyl molecule are suggested to be dissociated continuously due to the influence of metal catalysis and high temperature. Then bipyridyl molecule goes on reacting sequentially with further pyridine molecules until a layer nitrogen doped graphene forms on the catalyst surface. It can be seen that such N-doped graphene formed from pyridine contains only pyridine-like nitrogen atoms, implying that such formation method is feasible to produce N-doped graphene containing pure pyridine-like nitrogen atoms.

Slab model

We also calculated the adsorption configurations of pyridine on Ni(111) by using the slab model (Fig. 4) and the corresponding adsorption geometry parameters are shown in Table 4. It is seen that the binding energies of the adsorption configurations are in the same sequence as those for the cluster model although the binding energies obtained by the cluster

Table 4 The adsorption geometry of pyridine, bipyridyl and pyridyl radical on Ni(111) surface (slab model)

System	Site	E_{ad}[a]/eV	d_z[b]/Å	d_{C-C}[c]/Å	d_{C-N}[c]/Å	d_{N-Ni}[c]/Å	θ[d]/°	φ[d]/°
Pyridine (Fig. 4c)	Top	1.31	1.97	1.396	1.353	2.08	0	90
Bipyridyl (Fig. 4c)	Bridge	4.02	1.97	1.427, 1.453, 1.438	1.394, 1.399	1.98	10	0
$C_5NH_4^{\bullet}$ + $H^{\bullet}$ (Fig. 4c)	Bridge	5.93	1.57	1.390, 1.410	1.402, 1.363	2.082	0	60
$C_5NH_4^{\bullet}$ + $H^{\bullet}$ + C_5NH_5 (Fig. 4c)	Bridge (L)	7.60	1.851	1.395, 1.410	1.348	1.865	—	60
	Top (R)	—	1.974	1.394, 1.397	1.354	—	—	90
$2C_5NH_4^{\bullet}$ + $2H^{\bullet}$ (Fig. 4f)	Bridge (L)	12.42	1.830	1.393, 1.407	1.365	1.904	—	90
	Bridge (R)	—	1.833	1.393, 1.397	1.349	1.873	—	90

[a] E_{ad} denotes adsorption energy. [b] d_z denotes the distance between adsorbate molecule and metal surface. [c] d_{C-C}, d_{C-Ni} and d_{N-Ni} denote the N–Ni lengths, respectively. [d] θ denotes the out-of-plane tilt angle of H atoms in adsorbate molecule. [e] φ denotes the angle between the adsorbate molecule plane and metal surface.

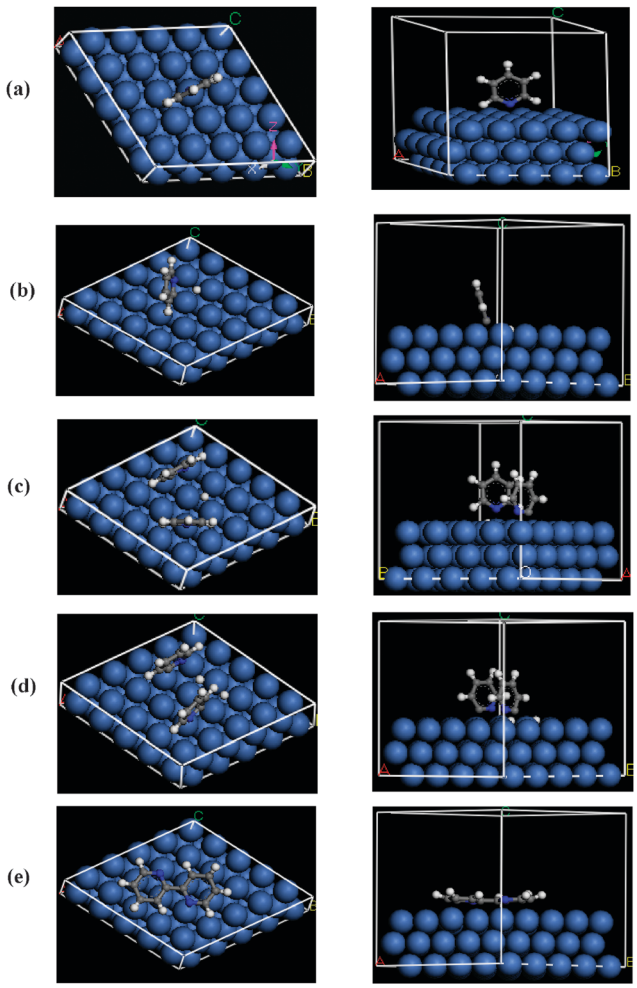

Fig. 4 Optimized geometry structure of the reactant, intermediate states and product of the whole reaction pathways for pyridine molecule dehydrogenate on Ni(111) surface to form bipyridyl by slab models, the top view and the side view is shown in right and left figure.

model are slightly lower than those by slab model, and corresponding adsorption geometry parameters are very similar to each other for the two models (Table 4).

Conclusions

In summary, the radical formation mechanism of bipyridyl molecule catalyzed by metal with pyridine precursor was studied using density functional theory calculations. This study is motivated by the possible synthesis of N-doped graphene from pyridine since similar synthesis for graphene can be conducted experimentally and the formation of bipyridyl can be considered as the initial process of the nitrogen doped graphene growth. The minimum energy path on the formation of bipyridyl on Ni(111) surface from two pyridine molecules has been shown to occur as follows: Step 1: the first pyridine molecule adsorbed on Ni surface dehydrogenates to form a pyridyl radical and a hydrogen radical. Step 2: the second pyridine molecule adsorbed on Ni surface dehydrogenates to form another pyridine radical and hydrogen radical. Step 3: the pyridyl radicals combine to form bipyridyl and hydrogen radicals combine to form an H_2 molecule. The results indicate that bipyridyl can be formed by two pyridines through dehydrogenation with a relatively low energy barrier, implying that the N-doped graphene can be synthesized by pyridine at a relatively low temperature. We expect that an experimental synthesis of N-doped graphene from pyridine precursor at a relatively low temperature could be carried out in future.

Acknowledgements

This work was financially supported by NSFC (No. 21005073) and Zhejiang Normal University (No. KJ20090121 and KJ20090117), and we also thank Prof. Zheng Hu for his valuable direction.

Notes and references

1 K. S. Novoselov, A. K. Geim, S. V. Morozov, D. Jiang, Y. Zhang, S. V. Dubonos, I. V. Grigorieva and A. A. Firsov, *Science*, 2004, **306**, 666; K. S. Novoselov, A. K. Geim, S. V. Morozov, D. Jiang, M. I. Katsnelson, I. V. Grigorieva, S. V. Dubonos and A. A. Firsov, *Nature*, 2005, **438**, 197; A. K. Geim and K. S. Novoselov, *Nat. Mater.*, 2007, **6**, 183; H. B. Heersche, P. Jarillo-Herrero, J. B. Oostinga, L. M. K. Vandersypen and A. F. Morpurgo, *Nature*, 2007, **446**, 56; J. R. Williams, L. DiCarlo and C. M. Marcus, *Science*, 2007, **317**, 638.
2 A. Charrier, A. Coati, T. Argunova, F. Thibaudau, Y. Garreau, R. Pinchaux, I. Forbeaux, J.-M. Debever, M. Sauvage-Simkin and J.-M. Themlin, *J. Appl. Phys.*, 2002, **92**, 2479.
3 K. S. Novoselov, D. Jiang, F. Schedin, T. J. Booth, V. V. Khotkevich, S. V. Morozov and A. K. Geim, *Proc. Natl. Acad. Sci. U. S. A.*, 2005, **102**, 10451.
4 D. A. Dikin, S. Stankovich, E. J. Zimney, R. D. Piner, G. H. B. Dommett, G. Evmenenko, S. T. Nguyen and R. S. Ruoff, *Nature*, 2007, **448**, 457; S. Stankovich, D. A. Dikin, R. D. Piner, K. A. Kohlhaas, A. Kleinhammes, Y. Jia, Y. Wu, S. T. Nguyen and R. S. Ruoff, *Carbon*, 2007, **45**, 1558; Y. Zhou, Q. Bao, L. A. L. Tang, Y. Zhong and K. P. Loh, *Chem. Mater.*, 2009, **21**, 2950.
5 W. Zhang, J. Cui, C. Tao, Y. Wu, Z. Li, L. Na, Y. Wen and G. Li, *Angew. Chem., Int. Ed.*, 2009, **48**, 5864.
6 D. Wei, Y. Liu, Y. Wang, H. Zhang, L. Huang and G. Yu, *Nano Lett.*, 2009, **9**, 1752.
7 Y. Wang, Y. Shao, D. W. Matson, J. Li and Y. Lin, *ACS Nano*, 2010, **4**, 1790.
8 L. Qu, Y. Liu, J. Baek and L. Dai, *ACS Nano*, 2010, **4**, 1321.
9 A. L. M. Reddy, A. Srivastava, S. R. Gowda, H. Gullapolli, M. Dubey and P. M. Ajayan, *ACS Nano*, 2010, **4**, 6337.
10 U. A. Palnitkar, R. V. Kashid, M. A. More, D. S. Joag, L. S. Panchakarla and C. N. R. Rao, *Appl. Phys. Lett.*, 2010, **97**, 063102.
11 L. Zhang, X. Liang, W. Song and Z. Wu, *Phys. Chem. Chem. Phys.*, 2010, **12**, 12055.
12 R. Sen, B. C. Satishkumar, A. Govindaraj, K. R. Harikumar, G. Raina, J. P. Zhang, A. K. Cheetham and C. N. R. Rao, *Chem. Phys. Lett.*, 1998, **287**, 671; M. Nath, B. C. Satishkumar, A. Govindaraj, C. P. Vinod and C. N. R. Rao, *Chem. Phys. Lett.*, 2000, **322**, 333.
13 H. Feng, J. Ma and Z. Hu, *J. Mater. Chem.*, 2010, **20**, 1702.
14 Y. Tian, Z. Hu, Y. Yang, X. Z. Wang, X. Chen, H. Xu, Q. Wu, W. J. Ji and Y. Chen, *J. Am. Chem. Soc.*, 2004, **126**, 1180.
15 H. Feng, J. Ma and Z. Hu, *J. Phys. Chem. C*, 2009, **113**, 16495.
16 B. Delley, *J. Chem. Phys.*, 1990, **92**, 508; B. Delley, *J. Phys. Chem.*, 1996, **100**, 6107; B. Delley, *J. Chem. Phys.*, 2000, **113**, 7756.
17 T. A. Halgren and W. N. Lipscomb, *Chem. Phys. Lett.*, 1977, **49**, 225.
18 X. D. Liu, H. Y. Zhang, K. Lu and Z. Q. Hu, *J. Phys.: Condens. Matter*, 1994, **6**, L497.
19 M. R. Cohen and R. P. Merrill, *Langmuir*, 1990, **6**, 1282.

 This journal is © the Owner Societies 2011